Surface Charge Density Determination of Single Conical Nanopores Based on Normalized Ion Current Rectification

ARTICLE *in* LANGMUIR · DECEMBER 2011

Impact Factor: 4.46 · DOI: 10.1021/la203106w · Source: PubMed

7 AUTHORS, INCLUDING:

Juan Liu
University of Maryland, Baltimore County
13 PUBLICATIONS **109** CITATIONS

SEE PROFILE

Jingyu Feng
Firmenich
6 PUBLICATIONS **76** CITATIONS

SEE PROFILE

Surface Charge Density Determination of Single Conical Nanopores Based on Normalized Ion Current Rectification

Journal:	*Langmuir*
Manuscript ID:	la-2011-03106w.R1
Manuscript Type:	Article
Date Submitted by the Author:	n/a

Complete List of Authors:	Liu, Juan; Georgia State University, chemistry Kvetny, Maksim; Georgia State University, chemistry FENG, JINGYU; GSU Wang, Dengchao; Georgia State University, Chemistry Wu, Baohua Brown, Warren; Georgia State University, chemistry Wang, Gangli; Georgia State University, Department of Chemistry

Surface Charge Density Determination of Single Conical Nanopores Based on Normalized Ion Current Rectification

Juan Liu, Maksim Kvetny, Jingyu Feng, Dengchao Wang, Baohua Wu, Warren Brown, Gangli Wang*
Department of Chemistry, Georgia State University, Atlanta, Georgia 30302
RECEIVED DATE (automatically inserted by publisher); E-mail: glwang@gsu.edu

Abstract: Current rectification is well-known in ion transport through nanoscale pores and channel devices. The measured current is affected by both the geometry and fixed interfacial charges of the nanodevices. In this paper, an interesting trend is observed in steady-state current-potential measurements using single conical nanopores. A threshold low conductivity state is observed upon the dilution of electrolyte concentration. Correspondingly, the normalized current at positive bias potentials drastically increases and contributes to different degree of rectification. The novel opposite trend at opposite bias polarities is employed to differentiate the ion flux affected by the fixed charges at the substrate-solution interface (surface effect), with respect to the constant asymmetric geometry (volume effect). The surface charge density (SCD) of individual nanopores, an important physical parameter that is challenging to measure experimentally and is known to vary from one nanopore to another, are directly quantified by solving Poisson and Nernst-Planck equations in the simulation of the experimental results. Flux distribution inside the nanopore and SCD of individual nanopores are reported. The respective diffusion and migration translocations are found to vary at different positions inside the nanopore. The knowledge is believed important for resistive pulse sensing applications, as the detection signal is determined by the perturbation of ion current by the analytes.

Introduction

Fundamental transport properties in individual synthetic nanopores and nanochannel devices have attracted extensive research interests.[1-8] Unique mass transport (MT) behaviors at high surface-volume-ratio render the synthetic nanopores and nanochannels promising platforms as rapid and lower-cost analytical sensors.[9-13] With a nanopore or nanochannel connecting two solution reservoirs through which a bias potential is applied, the nanopore region limits the ionic transport process thus the overall conductivity. As both nanoscale geometry (radius, length, etc.) and interface (coulombic interaction between fixed surface charges and mobile ions in solution) affect the ion transport signal, the overall current or conductance measured experimentally does not reveal the respective impacts of surface and volume factors. The knowledge is important for quantitative sensing applications, as the analytes perturb those factors differently at different regions of the nanodevices and generate signals differently.

The MT resistance of a nanopore is not a constant value at different applied potentials, which cause the measured current-voltage (i-V) curve to deviate from linearity (Ohm's law). The current at one potential polarity is often different from that at the same amplitude but opposite potential polarity, well known as ion current rectification (ICR).[14,15] The deviation from linear Ohmic behavior is generally believed a consequence of the asymmetric geometry and charge distribution at the nanoscale interface. The asymmetric device geometry, and asymmetry between radial influx and pseudo-planar efflux at the opening region, are referred as *volume effects* in this paper. At high surface to volume ratio, the transport of cations and anions are significantly affected by coulombic interaction with the fixed charges at the

substrate-solution interface, referred as surface effects. The concept is illustrated in Scheme 1.

A quantitative correlation of the measured ICR with the physical parameters of the nanodevices, specifically surface charge density (SCD) that establishes the surface electrical field inside nanopore, has not been established experimentally. The fixed charges at substrate-solution interface inside nanopore have opposite impacts on the transport of cation and anion via columbic interaction. The density of fixed charges at the solid-solution interface is fundamentally important for sensing applications and directly affects the electrochemical energy conversion in high energy density devices.[1,16,17] The knowledge of SCD within nanodevices is generally extrapolated from the values obtained from bulk measurements, which varies widely in the literature and is known to depend on measurement conditions.[18] Direct experimental determination of SCD at nanometer scale of individual nanodevices remains a challenge. Average SCD values from flat surface are frequently used in theoretical approaches. However, it is well known that the efficacy and responses of individual nanodevices used in experiments vary from one to another, depending on measurement conditions.

At present the transport behaviors are mostly studied experimentally by time domain conductivity measurements at constant or scanning potentials. The measured ionic current, carried by cation and anion transport, reflects both volume and surface impacts. This convoluted overall current-potential behaviors has led to several qualitative models summarized in recent reviews.[14,15,19] Briefly, the rectification behavior has been explained by potential ratchet, inhomogeneous conductivity, or ion mobility differences at nanopore region

due to the combined volume and surface effects. Analytical and numeric simulation based on Poisson, Nernst-Planck and Navier-Stokes equations have been reported to describe the overall conductivity through nanopores and nanochannels of various geometry.[20-26] While those models describe the experimental trend correctly, they often fail to explain the different degree of ICR observed experimentally from the same types of substrate materials with comparable geometry.

In stochastic nanopore sensing based on Coulter Counter concept,[27-32] the binding and transport of analytes perturb the ion flux and generate the current signal. Volume effects (size of analytes over nanopore volume) are routinely considered in the analysis, with the prerequisites of uniform flux distribution inside the nanopore and negligible surface effects. Experimentally, the efficacy of the nanosensors varies from one to another, which is generally postulated to the heterogeneity of the fabrication and functionalization process. Non-invasive characterization of individual nanosensors, both geometry and surface features, is critical for broad applications but is a significant challenge to address.

Our recent AC impedance analysis has revealed ion transport processes with different time constants, with the physical origin attributed to volume and surface impacts.[33] The experimental evidences that reveal: 1. spatial distribution of ion flux in addition to ion concentration at the nanopore region; 2. respective volume and surface impacts on the ionic transport process; and 3. respective contribution of cation and anion to the overall measured ionic current, will greatly advance the fundamental understanding of the transport phenomenon. In this report, combined experimental and theoretical approach is employed to differentiate the volume and surface effects in ion transport through single conical nanopores.

By normalizing the current-voltage responses measured from high to low ion concentrations, surface effects via columbic interaction are found to enhance the conductivity at positive bias potentials (outside vs. inside). A threshold normalized conductivity was observed at low conductivity states upon dilution. This opposite trend differentiates surface effects from geometric parameters that normally have the same impacts at both potential polarities. Direct characterization of SCD of individual nanopores is achieved by fitting the experimental results with continuum theory.

EXPERIMENTAL SECTION

Materials. Water (~18.2 MΩ• cm) is purified by a Barnstead E-pure water purification system. All other chemicals and materials were used as received. Corning 8161 glass capillaries (OD 1.50 mm, ID 1.10 mm) were from Warner Instruments and Tungsten rods from A-M System, Inc. Platinum wire (99.95%, diameter 25 μm), silver conductive paste, silver wire (99.9985%, diameter 0.5 mm), ferrocene were from Alfa Aesar. KCl was from J. T. Baker. $CaCl_2$, $FeCl_3$ (97%), HNO_3, H_2SO_4, H_2O_2 (30%), acetone, acetonitrile, tetrabutylammonium perchlorate (TBAP) were from Sigma-Alrich. 3-aminopropyldimethyl-ethoxysilane was from Gelest Inc.

Conical Nanopore Fabrication and Surface Modification The fabrication of glass nanopores followed previous reports.[7,33,34] Briefly, one end of a 25 μm Pt wire was electrochemically etched to create a sharpened nanotip. The sharpened Pt tip was then sealed inside a glass capillary. Excess glass was manually polished using sand papers and 50-nm-Al_2O_3 nanoparticles (from Alfa Aesar) sequentially till the nanotip was exposed. After

that, the exposed Pt nanotip inside glass shroud was electrochemically etched again, followed by mechanical pulling from the other end. Full removal of Pt wire inside the glass capillary results a through conical nanopore, with the length of ca. 10-20 μm and the shape replicating that of Pt nanotip. The nanopore structure has been extensively characterized by imaging and electrochemical methods in previous reports thus not shown in this paper.[7,33,34] After a nanopore was fabricated, it was rinsed with H_2O, EtOH and H_2O sequentially. Prior to silane modification, the glass surface was activated in 1 M HNO_3 for 15 minutes. After thorough rinsing with H_2O, EtOH and CH_3CN, the nanopore was loaded and soaked in 2% (v/v) 3-aminopropyldimethyl-ethoxy silane acetonitrile solution overnight. The modification by mono-ethoxy-silane is found to stabilize the electrochemical responses in the measurements based on previous studies.[33] The surface coverage is at ca. 20% based on those estimated from bulk measurements (Gelest).

Electrochemical Measurements A Gamry Reference 600 potentiostat was used in the conductivity studies (cyclic voltammetry software). The scan rate was generally at 20 mV/s. Two Ag/AgCl wires were used to control the bias potential. As the nanopore region limits the detected current signals, the Faradic processes at the macroscopic Ag/AgCl wires are not discussed in the paper. Both reference and counter electrode leads were connected to the same Ag/AgCl electrode immersed inside the nanopore while the working electrode was outside in the bulk solution. The radius of the nanopore is determined based on the absolute current values at + 0.050 V and – 0.050 V in 1 M KCl, where the surface effect is more effectively screened by the high concentration of electrolytes.

Theoretical Simulation The simulation was performed by solving Poisson and Nernst-Planck equations using COMSOL Multiphysics 4.0a software. The geometry used in the simulation is shown in supporting information Figure SI-1. Boundary 5 represents the negatively charged interior glass surface of the conical nanopore. To minimize the computation expenses without affecting the charge distribution near the mass transport limiting region, negative charges are placed on the exterior surface represented by boundary 4, which is 20 times of the pore radius. Adaptive free triangular mesh element was used. The mesh size within 300 nm inside the nanopore orifice was limited to 0.01 nm in an attempt to minimize the simulation noise. Other mesh elements at the charged boundaries (4 & 5) were set to range from 0.3 nm to 0.6 nm to reach the best resolution within a reasonable time. Note the dimension is approaching the size of solvated ions, which is a fundamental limit of continuum theory. The following parameters were used at room temperature (298.13 K): density $\rho = 1000$ kg/m^3, viscosity $\eta = 1\text{x}10^{-3}$ Pa*s, relative dielectric constant $\varepsilon = 80$, Faraday constant F = 96485 C/mol. The diffusion coefficient of K^+ and Cl^- in each concentration was listed in Table 1. Instead of using the number at infinite dilution, the values were corrected in each concentration by the transference number and measured conductivity. The details can be found in supporting information.

RESULTS AND DISCUSSION

Experiments: Normalized Conductivity in Potential Scanning Measurements

Conductivity measurements have been widely used to noninvasively characterize the dimension of nanodevices based on Ohm's law (resistance = solution factor times geometric factor).[35,36] The prerequisite is the negligible contribution from surface conductivity, which often leads to the increase of measured conductance therefore over-estimated size. Contrary to the symmetric nanochannels in which surface charges enhances the measured conductance at both potential polarities,[37] a novel trend was discovered in the normalized i-V curves in conical nanopore measurements, which allows the differentiation of surface and geometric effects. The i-V curves of a 26-nm-radius nanopore measured at different KCl concentrations were analyzed in Figure 1. The current amplitude in each curve was normalized by the corresponding concentration value to display the normalized conductivity. Almost linear ohmic behavior is observed in 1 M KCl (black) solution. When electrolyte concentration decreases from 1M, normalized current at positive potentials increases while that at negative potentials remain largely unchanged. Glass is negatively charged upon the deprotonation of surface silanol groups. The electrostatic interaction of mobile charge carriers (cation and anion) with those fixed surface charges is less screened at lower ionic strength. Since volume effect is determined by ohm's law, the deviation from linearity will reflect surface effects.

It is important to observe different trends at positive and negative potentials in the normalized conductivity plots. At positive potentials (outside vs. inside), the normalized current continues to increase as the electrolyte concentration decreases. At negative potentials, the almost overlapping current curves reveal a threshold normalized conductivity. As the increase of nanopore radius always results in the increase of current at both potential polarities, the opposite trend, especially the threshold low conductivity states, can be

employed to differentiate size and surface effects.

The deviation from linearity has been routinely quantified by the rectification factor (RF), which is the current ratio at an arbitrary potential value but opposite polarity (e.g. current at +0.4 V over current at -0.4 V). The increase of RF at low ionic strength can be explained by less screening of surface charge effects at low ionic strength, as the nanopore structure remain unchanged. The analysis suggests that at lower electrolyte concentration, ICR mainly originates from the enhanced conductivity at positive bias end. It also reveals a threshold low conductivity state, limited by the surface charge impacts on ion flux that is further discussed by simulation.

Similar trend was observed from other nanopores of different sizes (additional examples in Figure SI-2). The specific bulk concentration reaching apparent low current threshold varies from one GNP to another. Note the measured current reflects the non-Faradic transport of cations and anions through the nanopore. Due to the conical geometry, the smallest orifice region of the nanopore limits the transport process, while the impacts at the larger opening at the other end and the length of the nanopore are less significant and generally ignored in the literature and in this study.

Simulation based on Continuum Theory

The interesting trend of the normalized i-V curves reveals opposite impacts by surface effects on total conductivity at opposite bias potentials: enhanced and reduced conductivity at positive and negative bias potentials (outside vs. inside) respectively. The finding is in accordance with the AC impedance analysis previously reported by our group and by

molecular dynamic simulation.[33,38] To explain the observed phenomena and surface impacts quantitatively, the experimental results is fitted by classic theory simulation. Total ion flux is calculated through surface integration of flux at the exterior boundary electrode. The flux distribution inside nanopore is validated by the conservation of integrated flux at specified cutline position inside nanopore. While ion concentration inside different types of nanopores and nanochannels has been simulated (often under conditions different from experimental measurements),[20-25] the spatial distribution of ion flux at the nanopore region reveals interesting spatial variation of migration and diffusion contribution to the total flux. The information of ion flux distribution at the signal limiting nanopore region is more relevant to resistive pulse sensing applications, as the current signals being detected originate from the perturbation of ion flux by the analytes. The model geometry is described in experimental section and illustrated in supporting information Figure SI-1.

To gain an understanding of ion distribution and flux distribution at the signal limiting region, a cutline along radial direction at a designated depth (Z) inside the nanopore was introduced. The distribution of z-component flux and ionic concentration along the cutline were computed. The distance (R direction) is zero at the centerline and ends at the nanopore interior surface (boundary 5). As the applied bias potential is limited to a relatively low range, the contribution by electroosmotic flow is known to be small and ignored.[20-25] The model design was firstly validated by reproducing reported results,[20,39] in which the conductivity and ionic concentration along the centerline of a 50-nm-radius nanopore have been computed. The electric conductivity at + 0.4 V and – 0.4 V along the centerline of the 26-nm-radius nanopore is included in supporting information Figure SI-3. The variation of pore geometry

such as pore diameter and cone angle displays similar impacts as reported in literature. Representative results are included in Figure SI- 4.

I. Spatial Distribution of Ion Concentration Inside Nanopore The concentration profiles of K^+ and Cl^- along a 100-nm-cutline (radial direction) are shown in Figure 2. Within a few nanometers from the negatively charged glass surface at ±0.4 V potentials, K^+ is highly concentrated while the concentration of Cl^- is much lower due to electrostatic interactions. The concentration at the centerline can be seen in the inserted panel, which can be compared to those along the centerline, included in supporting information Figure SI-5. Unlike the general perception that cations are enriched while anions are repelled inside the nanopore by the negatively charged surface, interesting concentration profiles are observed at different potential polarities. At positive potentials where high conductivity states are observed experimentally, both the K^+ and Cl^- concentrations away from the charged surface are found to be higher than the defined bulk concentration of 50 mM (panel A). The high concentration of K^+ inside the pore is attributed to the radial influx of K^+ driven by the applied potential, which is also favored by the negatively charge surface via coulombic interaction. The high influx of K^+ ions in turn requires excess Cl^- to maintain the charge neutrality inside the nanopore. The intercepts on concentration axis at different cutlines are in agreement with the concentration profile in Figure SI-4, and in accordance with the trend along the centerline as previously reported.[20,22] The results suggest that anions also contributed to the higher conductivity in ICR, though to a less significant extent than cations. At -0.4 V bias potential (low conductivity states), the concentration away from the charged interface is lower than the

bulk concentration. In this case, the geometric factor, radial influx and pseudo-planar efflux (note the half cone angle is ca. 11°, scheme 1), tend to cancel the coulombic effects.

To provide a comprehensive view, the two-dimensional concentration profiles inside nanopore are shown in Figure 3. In each panel, the cross-section of the half-nanopore is projected at the bottom, with the pore orifice and centerline at zero for Z and R directions respectively. The concentration range differs in each panel for better observation of the spatial distribution. Accordingly, the high concentration of K^+ and low concentration of Cl^- ions near the charged interface were cut-off and displayed brush-like features. The results emphasize that anions are enriched to a different extent under high conductivity states in different regions of the nanopore. The absolute concentration value along the centerline can be found in supporting information Figure SI-5.

II. Spatial Distribution of Ion Flux Inside Nanopore Representative flux distributions of K^+ and Cl^- at 10-nm and 100-nm cutlines under the applied potentials of ±0.4 V are presented in Figure 4. At the vicinity of the nanopore interior surface, the z-direction flux of K^+ is much higher than that of Cl^-. This mainly results from the high concentration of K^+ due to coulombic interaction with the negatively charged nanopore surface. A few nanometers away from the boundary toward the centerline, the K^+ and Cl^- flux becomes comparable. The intercepts of the flux distribution at the centerline (R=0) can be seen in the inserted panel.

It is interesting to notice that the differences between the K^+ and Cl^- flux vary at different position and bias potentials (inserted panels), though the concentration profiles overlap away from the charged interface. The spatial variation of K^+ and Cl^- flux differences can be

explained by diffusion, driven by the concentration gradient. At positive bias potentials (outside vs. inside), ion concentration reaches maximum at ca. 100 nm inside the nanopore shown in Figure 3 and Figure SI-5. At 100-nm cutline, the concentration gradient is ca. zero. Therefore, no diffusion is expected and migration is the sole mechanism of ion flux. As the cutline is positioned near the orifice, concentration gradient increases. Importantly, the directions of diffusion and migration are the same for Cl^- flux, which increases the total Cl^- flux. Those of K^+ flux are opposite, causing the total K^+ flux to decrease. Consequently, the total flux of K^+ is less than that of Cl^- due to the cancellation effect at a certain spatial position that has the same concentration profile for both ions. The same rationale applies to any charged analyte in sensing applications. Correspondingly, the nature of the signal (i.e. current amplitude, duration) would depend on the binding location or transport trajectory.

To validate the flux distribution and to correlate with experimental i-V responses, the total flux through the cross-section of the nanopore at boundary and different Z position were computed by surface integration of flux distribution (R from zero to boundary 5). The total flux and current at the cutline ranging from 1 nm to 200 nm inside the nanopore has been computed with the results included in supporting information Table SI-1. As the conductivity was measured under steady-states, the total flux across the cross-section at any Z position should be conserved. This is confirmed by comparing the averaged flux values to the flux at the boundary electrode. It is worth pointing out that in continuum theory, the sizes of hydrated ions and ion-solvent interactions were not accounted for. Molecular level modeling would provide better fitting near the interface. Unfortunately its applicability is generally limited to the dimension of a few nanometers or less, therefore could not describe the overall

experimental behaviors of the nanopores used in this study.

III. Quantification of Effective SCD of Individual Nanopores While nanodevice geometry can be determined by various imaging techniques, non-invasive characterization of the interior surface is a challenge. With various nanostructures being developed for sensing and other applications, it is significant if the conductivity measurements could be employed to non-invasively quantify the SCD of individual nanodevices.

In aqueous solution, the SCD of glass substrate is mainly determined by the protonation/deprotonation of silanol groups (Si-OH). As the deprotonation process is associated with charge separation at the functional group, the pKa of those groups is known to be affected by the local surface electric field (surface morphology or geometry) and vary under different conditions.[18,40] Furthermore, glass is known to form a gel layer and respond to pH, the foundation of pH electrodes. Accordingly, SCD in this paper quantifies the accumulative fixed charges at the substrate-solution interface, from multi-layers instead of a monolayer of charges at the substrate surface.[41,42]

The experimental i-V responses were fitted by systematic variation of the SCD of the constructed nanopore. Shown in Figure 5, the simulated current (scattered points, total flux times Faraday's constant) matches the experimental i-V curve at ca. -170-240 mC/m^2 in different electrolyte concentrations at different potentials. In 1M KCl solution, the surface charge impacts become less obvious. All results at different SCD converge into the linear ohmic behavior and match the measured results well. As the electrostatic interaction with

charged interface becomes less screened at lower ion concentrations, ICR effects intensify. The simulated current at high conductivity states increases with the increase of SCD in a well defined fashion. The simulated current at low conductivity states displays rather weak dependence on SCD variation. Therefore, the determination of SCD in the following discussion is focused on high conductivity responses. Experimentally, the trend of low conductivity state current also varies from nanopore to nanopore in different electrolyte concentrations, attested by the results provided in Fig. SI-2. The offset between the simulated and measured low conductivity current is addressed in a separate study and does not affect the SCD determination. Again, the different trend, the increase of normalized conductivity at positive bias potentials and the threshold low conductivity, could not be fitted with the variation of geometric parameter.[43] In fact, the pore geometry is not expected to change in different electrolyte solutions.

To the best of our knowledge, no direct measurement of charge density has been reported at nanometer scale interface inside single nanodevices. The determined SCD is validated with the literature based on ensemble studies that actually have a wide range: from ca. -0.002e/nm^2 at low electrolyte concentration (μM range) up to ca. 1e/nm^2 (160 mC/m^2) at higher electrolyte concentrations.[18,40] The determined SCD at ca. 170-240 mC/m^2 is marginally higher but considered reasonable under the measurement conditions with high electric field. Glass is well known to form a gel layer in aqueous environment. The charge density in the gel layer is determined by the pKa of the functional groups in the SiO_2 network and solution pH. Note a high electric field could significantly facilitate the Si-O-H bond dissociation, which cause the variation of effective pKa values under different surface curvature.

Furthermore, recent reports suggest that deep hydration of glass surface could be as much as hundreds of nanometers,[44,45] which also supports the quantified effective SCD.

IV. Transference number of K^+ and Cl^- at high and low conductivity states The respective cationic (K^+) and anionic (Cl^-) contributions to the total current are summarized in Table 2. At +0.4 V (outside vs. inside), the normalized current of both K^+ and Cl^- increases as the concentration decreases. The high conductivity states are established with K^+ being the main charge carrier.[46] The low conductivity changes are much smaller and limited by both measurement uncertainty and simulation offset thus not discussed. At higher concentration (1M), the electrostatic interaction with the negatively charged interface is less obvious. The transference number of K^+ and Cl^- are comparable and primarily determined by their respective ion mobility (in reference to the bulk values listed in Table 1). The finite differences suggest that the ion strength at 1M is not sufficient to fully eliminate the surface effects at ±0.4 V for this nanopore. The normalized current of both ions significantly increase in more diluted solutions. With the normalized current in 1M representing volume conductivity, the differences in lower concentration quantifies the surface conductivity that leads to the high conductivity states.

The asymmetric nanopore geometry defines a radial influx of ions and pseudo-planar efflux. Note the ion species available within a certain mass transport distance is determined by the ion concentration on either side of the nanopore orifice. Divided by the cone angle (ca. 11°), the component of coulombic interaction along the Z direction directly affect ion current being detected, while the component along R direction change ion concentration and flux

distribution. At positive potentials (outside vs. inside), the radial K^+ influx is facilitated by the negatively charged nanopore interior surface. The migration of Cl^- ions under the applied potential is also enhanced by the surface effects, but the total Cl^- flux is less significant compared to K^+, as the efflux is planar and the Cl^- concentration is low near the interface. Therefore, the overall normalized current and K^+ transference number increase upon the dilution of electrolyte concentration. At negative potentials, the impacts by volume and surface potentials attenuate each other. The radial influx of Cl^- ions is repelled by the coulombic interaction with the negatively charge interface. The planar efflux of K^+ ions is also suppressed by surface effects. As the volume/geometric parameters are constant for individual nanopore, surface effects intensify upon the dilution of ion concentration. A threshold low conductivity state is established if surface effects reach maximum. If conventional double layer theory applies, this effect is expected if the double layer overlaps inside the nanopore. The specific concentration reaching this threshold current obviously depends on the size and surface charge density of individual nanopores.

Conclusion

Ion transport at single conical nanopores is investigated experimentally by conductivity measurements under scanning potentials, and theoretically through the simulation by solving Poisson and Nernst-Planck equations. The volume and surface charge effects are differentiated by normalizing the current-voltage responses measured at different ion concentrations. Surface effects via columbic interaction cancels the volume effects at negative, but enhances volume effects at positive bias potentials, leading to low or high

conductivity states in the measurements respectively. The SCD of individual nanopores are directly determined by fitting the experimental results with continuum theory. The spatial distribution of ion concentration and more importantly, ion flux distribution inside the nanopore, is reported. Correspondingly, the migration and diffusion contribution to the total flux is demonstrated to vary at different locations inside the nanopore. The flux distribution and its physical origin at the signal-limiting-nanopore-region are believed significant for sensing applications, as the magnitude and duration of the sensing signal depend on the location and trajectory of analytes (along the centerline vs. near the interface).

ACKNOWLEGMENT

The authors acknowledge Dr. Clemens Kubeil and Dr. Andrews Bund for providing their original Comsol model file for comparison. The discussion with Prof. Rui Qiao is acknowledged. The startup fund provided by Georgia State University is acknowledged. G. W. and J. L. were supported as part of the Fluid Interface Reactions, Structures and Transport (FIRST) Center, an Energy Frontier Research Center funded by the U.S. Department of Energy, Office of Science, Office of Basic Energy Sciences under Award Number ERKCC61.

SUPPORTING INFORMATION AVAILABLE

The simulation details and nanopore geometry; The averaged simulated current at different cutlines; The normalized CV of other nanopores; Conductivity along center line of the 26-nm-radius nanopore; Concentration profiles along centerline; Flux distribution at 1-nm

and 100-nm cutlines. Material is available free of charge via the Internet at http://pubs.acs.org.

REFERENCE

(1) Dekker, C. *Nat. Nanotechnol.* **2007**, *2*, 209.

(2) Schoch, R. B.; Han, J.; Renaud, P. *Rev. Mod. Phys.* **2008**, *80*, 839.

(3) Stein, D.; Kruithof, M.; Dekker, C. *Phys. Rev. Lett.* **2004**, *93*, 035901.

(4) Woermann, D. *PCCP* **2004**, *6*, 3130.

(5) Vlassiouk, I.; Siwy, Z. S. *Nano Lett.* **2007**, *7*, 552.

(6) Wanunu, M.; Meller, A. *Nano Lett* **2007**, *7*, 1580.

(7) Wang, G.; Zhang, B.; Wayment, J. R.; Harris, J. M.; White, H. S. *J. Am. Chem. Soc.* **2006**, *128*, 7679.

(8) Kovarik, M. L.; Zhou, K. M.; Jacobson, S. C. *J. Phys. Chem. B* **2009**, *113*, 15960.

(9) Deamer, D. W.; Branton, D. *Acc. Chem. Res.* **2002**, *35*, 817.

(10) Gu, L. Q.; Braha, O.; Conlan, S.; Cheley, S.; Bayley, H. *Nature* **1999**, *398*, 686.

(11) Branton, D.; Deamer, D. W.; Marziali, A.; Bayley, H.; Benner, S. A.; Butler, T.; Di Ventra, M.; Garaj, S.; Hibbs, A.; Huang, X.; Jovanovich, S. B.; Krstic, P. S.; Lindsay, S.; Ling, X. S.; Mastrangelo, C. H.; Meller, A.; Oliver, J. S.; Pershin, Y. V.; Ramsey, J. M.; Riehn, R.; Soni, G. V.; Tabard-Cossa, V.; Wanunu, M.; Wiggin, M.; Schloss, J. A. *Nat Biotechnol* **2008**, *26*, 1146.

(12) Kovarik, M. L.; Jacobson, S. C. *Anal. Chem.* **2008**, *80*, 657.

(13) Lan, W. J.; Holden, D. A.; Zhang, B.; White, H. S. *Anal. Chem.* **2011**, *83*, 3840.

(14) Siwy, Z. S.; Howorka, S. *Chem. Soc. Rev.* **2010**, *39*, 1115.

(15) Daiguji, H. *Chem Soc Rev* **2010**, *39*, 901.

(16) Long, J. W.; Dunn, B.; Rolison, D. R.; White, H. S. *Chem. Rev.* **2004**, *104*, 4463.

(17) Murray, R. W. *Chem. Rev.* **2008**, *108*, 2688.

(18) Behrens, S. H.; Grier, D. G. *J. Chem. Phys.* **2001**, *115*, 6716.

(19) Siwy, Z. S. *Adv. Funct. Mater.* **2006**, *16*, 735.

(20) White, H. S.; Bund, A. *Langmuir* **2008**, *24*, 2212.

(21) Vlassiouk, I.; Smirnov, S.; Siwy, Z. *Acs Nano* **2008**, *2*, 1589.

(22) Cervera, J.; Schiedt, B.; Ramirez, P. *Europhys. Lett.* **2005**, *71*, 35.

(23) Ai, Y.; Zhang, M.; Joo, S. W.; Cheney, M. A.; Qian, S. *The Journal of Physical Chemistry C* **2010**, *114*, 3883.

(24) Qian, S.; Joo, S. W.; Ai, Y.; Cheney, M. A.; Hou, W. *J Colloid Interface Sci* **2009**, *329*, 376.

(25) Wang, X.; et al. *J. Phys. D: Appl. Phys.* **2007**, *40*, 7077.

(26) White, H. S.; Bund, A. *Langmuir* **2008**, *24*, 12062.

(27) Ito, T.; Sun, L.; Henriquez, R. R.; Crooks, R. M. *Acc. Chem. Res.* **2004**, *37*, 937.

(28) Sexton, L. T.; Horne, L. P.; Sherrill, S. A.; Bishop, G. W.; Baker, L. A.; Martin, C. R. *J. Am. Chem. Soc.* **2007**, *129*, 13144.

(29) Fologea, D.; Brandin, E.; Uplinger, J.; Branton, D.; Li, J. *Electrophoresis* **2007**, *28*, 3186.

(30) Vlassiouk, I.; Kozel, T. R.; Siwy, Z. S. *J Am Chem Soc* **2009**, *131*, 8211.

(31) Talaga, D. S.; Li, J. *J Am Chem Soc* **2009**, *131*, 9287.

(32) Lemay, S. G. *Acs Nano* **2009**, *3*, 775.

(33) Feng, J.; Liu, J.; Wu, B.; Wang, G. *Analytical Chemistry* **2010**, *82*, 4520.

(34) Zhang, B.; Galusha, J.; Shiozawa, P. G.; Wang, G.; Bergren, A. J.; Jones, R. M.; White, R. J.; Ervin, E. N.; Cauley, C. C.; White, H. S. *Anal. Chem.* **2007**, *79*, 4778.

(35) Li, N. C.; Yu, S. F.; Harrell, C. C.; Martin, C. R. *Anal. Chem.* **2004**, *76*, 2025.

(36) Sakmann, B.; Neher, E. *Single-channel recording*; 2nd ed.; Plenum Press: New York, 1995.

(37) Karnik, R.; Fan, R.; Yue, M.; Li, D.; Yang, P.; Majumdar, A. *Nano Lett* **2005**, *5*, 943.

(38) Krems, M.; Pershin, Y. V.; Di Ventra, M. *Nano Lett.* **2010**, *10*, 2674.

(39) Kubeil, C.; Bund, A. *J. Phys. Chem. C* **2011**, *115*, 7866.

(40) Iler, R. K. *The chemistry of silica : solubility, polymerization, colloid and surface properties, and biochemistry*; Wiley: New York, 1979.

(41) Velmurugan, J.; Zhan, D.; Mirkin, M. V. *Nat Chem* **2010**, *2*, 498.

(42) Zhan, D.; Velmurugan, J.; Mirkin, M. V. *Journal of the American Chemical Society* **2009**, *131*, 14756.

(43) Ramirez, P.; Apel, P. Y.; Cervera, J.; Mafe, S. *Nanotechnology* **2008**, *19*, 315707.

(44) Li, Y.; Bergman, D.; Zhang, B. *Anal. Chem.* **2009**, *81*, 5496.

(45) Sun, P.; Mirkin, M. V. *J Am Chem Soc* **2008**, *130*, 8241.

(46) Jorne, J. *Nano Lett.* **2006**, *6*, 2973.

Table 1 The diffusion coefficient of K^+ and Cl^- ions in different KCl solution.*

Conc.(M)	Conductivity (S/m)	t_{K^+}	t_{Cl^-}	K^+ conductivity (S/m)	Cl- conductivity (S/m)	Effective D_{K+} (m^2/s)	Effective D_{Cl-} (m^2/s)
0.0500	0.667	0.4899	0.5101	0.327	0.340	1.740e-9	1.812e-9
0.100	1.290	0.4898	0.5102	0.631	0.657	1.680e-9	1.750e-9
1.00	11.19	0.4882	0.5118	5.463	5.727	1.455e-9	1.525e-9

* The solution conductivity and ion transference number are from "Electrolyte Solutions", Second edition, by Robinson and Stokes (table 7.7 on page 158; and Appendix 6.3 on page 466).

Table 2 Summary of simulated K^+ and Cl^- contribution to the transport current.*

Conc.(M)	E (V)	Measured i (nA)	K^+ Current (nA)	Cl^- Current (nA)	Total simulated i (nA)	t_{K^+}	t_{Cl^-}	Norm. K^+ current (by conc.)	Norm. Cl^- current (by conc.)
0.0500	0.40	8.84	5.1	3.1	8.23	0.62	0.38	102	62.0
0.100	0.40	13.8	8.3	5.6	13.9	0.60	0.40	83.0	56.0
1.00	0.40	66.8	34.3	33.6	67.9	0.51	0.49	34.3	33.6

* The simulated current and corresponding transference number listed in this table are based on the SCD that best fit the experiments in each concentration.

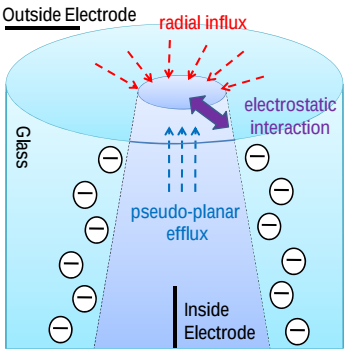

Scheme 1. Ion flux confined by nanopore geometry and interaction with the fixed charges at glass-solution interface. Double arrow suggests the electrostatic interaction between mobile ions and those fixed negative charges, which can be devided into two components along and normal to the direction of ion flux. Not drawn to scale.

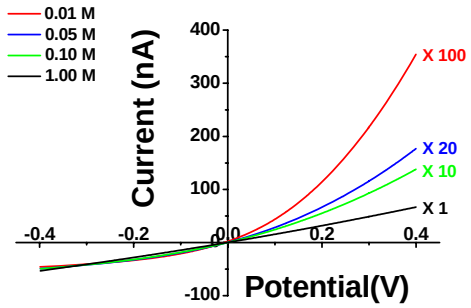

Figure 1. Normalized conductivity plots of a 26-nm-radius nanopore in different KCl solutions. The current was normalized based on concentration, with the factor listed next to each curve (red 0.01 M, X100; blue 0.05 M, X20; green 0.10 M, X10; black 1.00 M, X1). Scan rate was at 20 mV/s.

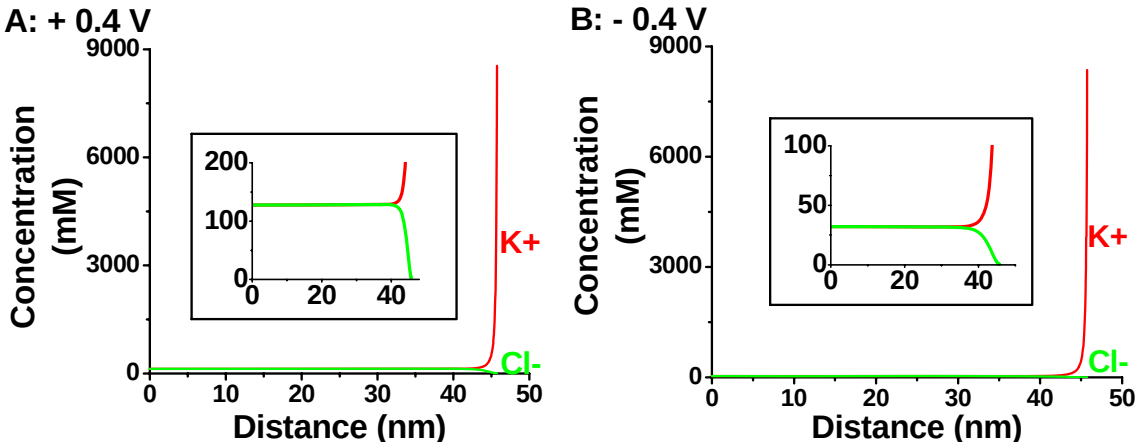

Figure 2. Concentration profiles of K^+ (red) and Cl^- (green) at **A:** + 0.4 V; and **B:** -0.4 V at cutline z = -100 nm. The x axis represents the distance away from the centerline along the cutline. The radius of the nanopore is set at 26-nm with surface charge density defined at -170 mC/m^2 (value based on Figure 7). The bulk concenstrion of KCl is 50 mM. The intercept on the concentration axis is enlarged in the inserted panel.

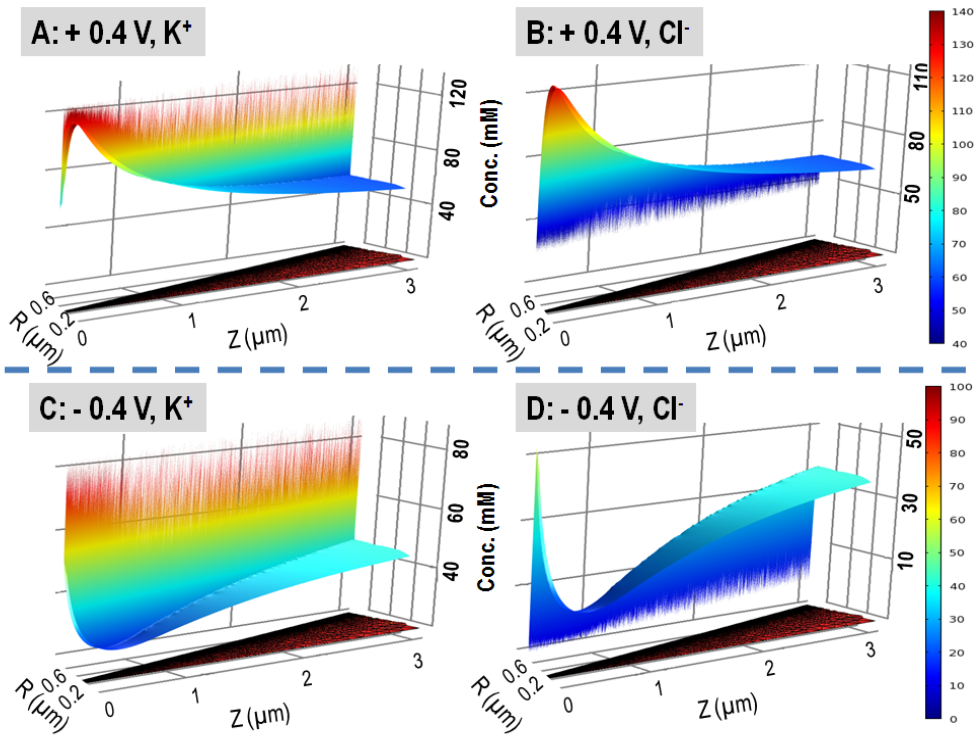

Figure 3. Spatial distribution of K^+ and Cl^- concentrations inside nanopore for a 26 nm GNP in 50 mM KCl with -170 mC/m^2 SCD. The half-cross-section nanopore geometry is shown at the bottom of each panel. The adaptive mesh elements are much denser near the charged interface (boundary 5). The nanopore orifice is at Z=0 nm and centerline is at R=0 nm. The concentration profiles inside the nanopore at 3 μm and beyond continuously extend those features shown thus not included. The top color scale applies to panel A and B, while the bottom one applies to panel C and D. Note the brush-like features near the interface resulted from the cut-off concentration range, which was set during the plotting for better view. The absolute values at representative positions can be found in Figure 2 and Figure SI-4.

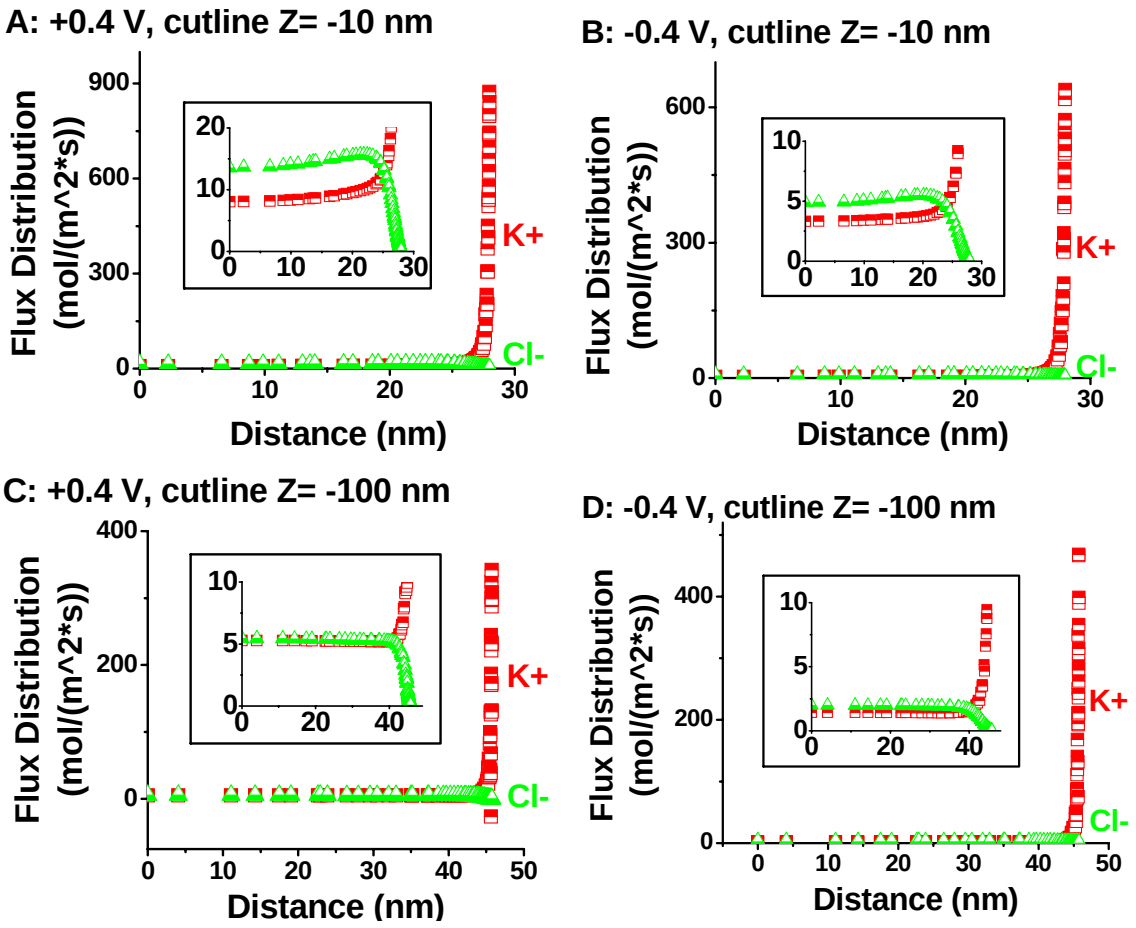

Figure 4 Flux distribution of K^+ (red square) and Cl^- (green triangle) at **A:** + 0.4 V; and **B:** -0.4 V at cutline z = -10 nm: **C:** + 0.4 V; and **D:** -0.4 V at cutline z = -100 nm The x axis represents the distance away from the centerline along the cutline. The radius of the nanopore is set at 26-nm with surface charge density defined at -170 mC/m^2 (value based on Figure 7). The bulk concentration of KCl is 50 mM. The intercept on the flux density axis is enlarged in the inserted panel.

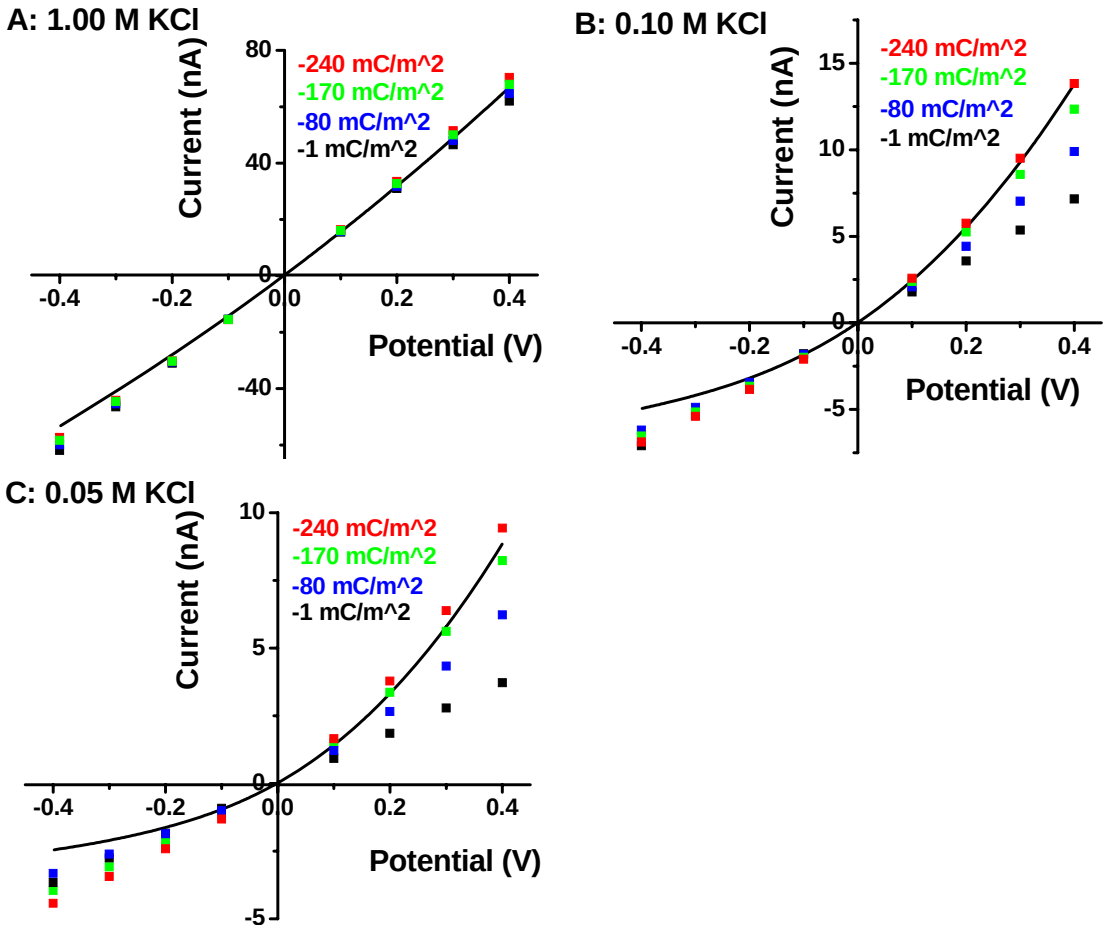

Figure 5. Measured conductivity (black solid line) from a ca. 26-nm-radius nanopore in KCl solution with different concentration. Simulation results for a 26 nm in 1.00 M (panel A); 0.10 M (panel B); 0.05 M (panel C) KCl solutions with different SCD indicated in panels.

FOR TOC ONLY

Surface charge density determination of individual nanopores